Boundary-Layer Meteorol (2009) 133:139–164
DOI 10.1007/s10546-009-9424-0

ARTICLE

Energy- and Flux-Budget Turbulence Closure Model for Stably Stratified Flows. Part II: The Role of Internal Gravity Waves

S. S. Zilitinkevich · T. Elperin · N. Kleeorin · V. L'vov · I. Rogachevskii

Received: 10 May 2009 / Accepted: 27 August 2009 / Published online: 22 September 2009

Abstract We advance our prior energy- and flux-budget (EFB) turbulence closure model for stably stratified atmospheric flow and extend it to account for an additional vertical flux of momentum and additional productions of turbulent kinetic energy (TKE), turbulent potential energy (TPE) and turbulent flux of potential temperature due to large-scale internal gravity waves (IGW). For the stationary, homogeneous regime, the first version of the EFB model disregarding large-scale IGW yielded universal dependencies of the flux Richardson number, turbulent Prandtl number, energy ratios, and normalised vertical fluxes of momentum and heat on the gradient Richardson number, *Ri*. Due to the large-scale IGW, these dependencies lose their universality. The maximal value of the flux Richardson number (universal constant $\approx$0.2–0.25 in the no-IGW regime) becomes strongly variable. In the vertically homogeneous stratification, it increases with increasing wave energy and can even exceed 1. For heterogeneous stratification, when internal gravity waves propagate towards stronger stratification, the maximal flux Richardson number decreases with increasing wave energy, reaches zero and then becomes negative. In other words, the vertical flux of potential temperature becomes counter-gradient. Internal gravity waves also reduce the anisotropy of turbulence: in contrast to the mean wind shear, which generates only horizontal TKE, internal gravity waves gener-

S. S. Zilitinkevich (✉)
Finnish Meteorological Institute, Helsinki, Finland
e-mail: sergej.zilitinkevich@fmi.fi

S. S. Zilitinkevich
Division of Atmospheric Sciences, University of Helsinki, Helsinki, Finland

S. S. Zilitinkevich
Nansen Environmental and Remote Sensing Centre/Bjerknes Centre for Climate Research, Bergen, Norway

T. Elperin · N. Kleeorin · I. Rogachevskii
Department of Mechanical Engineering, Pearlstone Centre for Aeronautical Engineering Studies, Ben-Gurion University of the Negev, Beer-Sheva, Israel

V. L'vov
Department of Chemical Physics, Weizmann Institute of Science, Rehovot, Israel

ate both horizontal and vertical TKE. Internal gravity waves also increase the share of TPE in the turbulent total energy (TTE = TKE + TPE). A well-known effect of internal gravity waves is their direct contribution to the vertical transport of momentum. Depending on the direction (downward or upward), internal gravity waves either strengthen or weaken the total vertical flux of momentum. Predictions from the proposed model are consistent with available data from atmospheric and laboratory experiments, direct numerical simulations and large-eddy simulations.

Keywords Internal gravity waves · Stable stratification · Turbulence closure · Turbulent energies · Vertical turbulent fluxes · Wave-induced transports

List of Symbols

$A_z = E_z/E_K$	Ratio of the vertical turbulent kinetic energy, E_z, to TKE, E_K
$E = E_K + E_P$	Total turbulent energy (TTE)
$E_K = \frac{1}{2}\langle u_i u_i \rangle$	Turbulent kinetic energy (TKE)
E_i	Vertical ($i = z$) and horizontal ($i = x, y$) components of TKE
$E_\theta = \frac{1}{2}\langle \theta^2 \rangle$	"Energy" of potential temperature fluctuations
E_P	Turbulent potential energy (TPE) given by Eq. 25
E_W	IGW kinetic energy given by Eq. 16
$\hat{E}_z$	Dimensionless vertical TKE given by Eq. 70
$\mathbf{e}$	Vertical unit vector
$e_W(\mathbf{k})$	Energy spectrum of the ensemble of internal gravity waves (IGW) given by Eq. 17
$F_i = \langle u_i\ \theta \rangle$	Potential-temperature flux
F_z	Vertical component of the potential-temperature flux
F_i^W	Instantaneous potential-temperature flux caused by the IGW–turbulence interaction given by Eq. 42
F_i^{WW}	Potential-temperature flux caused by IGW averaged over the period of IGW, given by Eq. 21
F_θ^W	Scale of the IGW contribution turbulent flux of potential temperature given by Eq. 57
$\hat{E}_z$	Dimensionless vertical TKE given by Eq. 70
$f = 2\Omega \sin\varphi$	Coriolis parameter
G	"Wave-energy parameter" proportional to the normalized IGW kinetic energy, E_W, given by Eq. 50
$\mathbf{g}$	Acceleration due to gravity
H	External height scale
K_M	Eddy viscosity given by Eq. 79
K_H	Eddy conductivity given by Eq. 80
$\mathbf{k}$	Wave vector
$k_\alpha = (k_x, k_y)$	Horizontal wave vector with $k_h = \pm\sqrt{k_x^2 + k_y^2}$
$k = \sqrt{k_z^2 + k_h^2}$	Total wavenumber
L	Obukhov length scale given by Eq. 5
L_W	Minimal wave length of the large-scale IGW
l_z	Vertical turbulent length scale
N	Mean-flow Brunt–Väisälä frequency

P	Pressure
P_0	Reference value of P
P^W	Pressure variation caused by IGW
p	Pressure fluctuation caused by turbulence
$Pr = \nu/\kappa$	Prandtl number
Pr_T	Turbulent Prandtl number given by Eq. 2
Q	Dimensionless lapse rate given by Eq. 44
Q_{ij}	Correlations between the pressure and the velocity-shear fluctuations, given by Eqs. 34 and 63
$\mathbf{r}$	Radius-vector of the centre of the wave packet
Ri	Gradient Richardson number, Eq. 1
Ri_f	Flux Richardson number, Eq. 4
Ri_f^∞	Limiting value of Ri_f in the flow without IGW (universal constant in the homogeneous sheared flow)
$Ri_f^{\max}$	Limiting value of Ri_f in the presence of IGW (depends on the G and Q)
$S = \lvert\partial\mathbf{U}/\partial z\rvert$	Vertical shear of the horizontal mean wind
T	Absolute temperature
T_0	Reference value of the absolute temperature
$t_T = l_z E_z^{-1/2}$	Turbulent dissipation time scale
t_τ	Effective dissipation time scale
$\mathbf{V}^W = \left(V_1^W, V_2^W, V_3^W\right)$	IGW velocity given by Eqs. 9–10
$V_0^W(\mathbf{k})$	IGW amplitude
$\mathbf{U} = (U_1, U_2, U_3)$	Mean wind velocity
$\mathbf{u}$	Turbulent velocity
Z_0	Height of the IGW source
$\beta = g/T_0$	Buoyancy parameter
$\gamma = c_p/c_v$	Ratio of specific heats
ε_K, ε_θ, $\varepsilon_i^{(F)}$ and $\varepsilon_{ij}^{(\tau)}$	Dissipation rates for E_K, E_θ, $F_i^{(F)}$ and τ_{ij}
$\varepsilon_{\alpha 3(\mathrm{eff})}(\alpha = 1, 2)$	Effective dissipation rates of the vertical turbulent fluxes of momentum
κ	Temperature conductivity
μ	Exponent of the energy spectrum of the ensemble of IGW
ν	Kinematic viscosity
Φ_K, Φ_θ and Φ_F	Third-order moments representing turbulent fluxes of E_K, E_θ and F_i
φ	Latitude
Π^W	IGW production of TKE given by Eq. 49
Π_i^W	IGW production of the vertical ($i = z$) and horizontal ($i = x, y$) components of TKE given by Eqs. 52–53
Π_θ^W	IGW production of E_θ given by Eq. 56
$\Pi_E^W = \Pi^W + \Pi_\theta^W \beta^2 N^{-2}$	IGW production of TTE
Π_F^W	IGW production of the flux of potential temperature given by Eq. 58
$\Pi_{\tau\alpha}^W$	IGW production of the non-diagonal components of the Reynolds stresses, $\tau_{\alpha 3}$, given by Eq. 61
τ_{ij}	Reynolds stresses characterising the turbulent flux of momentum

$\tau_{\alpha 3} (\alpha = 1, 2)$	Components of the Reynolds stresses characterising vertical turbulent flux of momentum
τ	Modulus of (τ_{13}, τ_{23})
τ_{ij}^{W}	Instantaneous Reynolds stresses caused by IGW, given by Eq. 41
τ_{ij}^{WW}	Reynolds stresses caused by IGW averaged over the period of IGW given by Eqs. 21 and 43
ρ_0	Density
Θ	Potential temperature
Θ^W	IGW potential temperature given by Eq. 11
θ	Turbulent fluctuation of potential temperature
Ω_i	Earth's rotation vector parallel to the polar axis
ω	Frequency of IGW

1 Introduction

Internal gravity waves (IGW) in relation to atmospheric and oceanic turbulence have been a subject of intense research [e.g., monographs: Beer (1974), Gossard and Hooke (1975), Baines (1995), Nappo (2002); and review papers: Garrett and Munk (1979), Fritts and Alexander (2003), Thorpe (2004), Staquet and Sommeria (2002)]. In the atmosphere, IGW are present at scales ranging from metres to kilometres, and are measured by direct probing or remote sensing using radars and lidars (Chimonas 1999; Fritts and Alexander 2003).

The sources of IGW are: strong wind shear, flows over topography, convective and other local-scale motions underlying the stably stratified layer (Wurtele et al. 1996; Fritts and Alexander 2003), geostrophic adjustment of unbalanced flows in the vicinity of jet streams and frontal systems, and wave–wave interactions (Staquet and Sommeria 2002; Fritts and Alexander 2003). The IGW propagation is complicated by variable wind speed and density profiles causing refraction, reflection, focusing, and ducting.

IGW contribute to the energy and momentum transport, the turbulence production and eventually enhance mixing. The dual nature of fluctuations representing both turbulence and waves in stratified flows has been recognised, e.g., by Jacobitz et al. (2005). The role of waves and the need for their inclusion in turbulence closure models has been discussed by Jin et al. (2003) and Baumert and Peters (2004, 2009). Baumert and Peters (2004) included an additional negative term in the TKE budget equation: the rate of transfer of TKE into potential energy of wave-like motions (highly irregular short internal waves coexisting with turbulent eddies), and postulated that with increasing stability these motions dominate random velocity and buoyancy fluctuations and suppress vertical mixing (see also Umlauf and Burchard 2005). The parameterization of mixing in the deep ocean due to short IGW was considered by Polzin (2004a,b). Finnigan and Einaudi (1981), Einaudi et al. (1984), Finnigan et al. (1984), Finnigan (1988, 1999), Einaudi and Finnigan (1993) analyzed the budgets of the wave kinetic energy and the wave temperature variance, and found significant buoyant production of the wave energy despite the strong static stability and energy transfer from waves to turbulence.

In the present paper we focus on the wave-induced vertical flux of momentum and the generation of turbulent kinetic energy (TKE), turbulent potential energy (TPE) and turbulent flux of potential temperature due to large-scale IGW in the context of an energetically consistent "energy- and flux-budget" (EFB) turbulence closure model for stably stratified flow

(Zilitinkevich et al. 2007, 2008). The model is designed for typical stably stratified atmospheric flows, characterised by the vertical shear $S = |\partial \mathbf{U}/\partial z|$ of the horizontal mean wind $\mathbf{U} = (U_1, U_2, 0)$, and is based on the budget equations for the key second moments: TKE, TPE, and the vertical turbulent fluxes of the momentum and the buoyancy (proportional to the potential temperature). It takes into account the non-gradient correction to the down-gradient formulation for the vertical turbulent flux of buoyancy, and employs the concept of total turbulent energy (TTE = TKE + TPE). It is a model without a critical Richardson number permitting sustenance of turbulence by shear at any gradient Richardson number

$$Ri = N^2/S^2, \tag{1}$$

where, N is the Brunt–Väisälä frequency defined as $N^2 = \beta \partial \Theta/\partial z$, Θ is the mean potential temperature, $\beta = g/T_0$ is the buoyancy parameter, g is the acceleration of gravity, and T_0 is the reference value of the absolute temperature T. For the turbulent Prandtl number, defined as

$$Pr_T = K_M/K_H, \tag{2}$$

where K_M and K_H are the eddy viscosity and eddy conductivity, the EFB model predicts the asymptotically linear dependence:

$$Pr_T \propto Ri \text{ at } Ri >> 1. \tag{3}$$

In terms of the flux Richardson number, Ri_f, and the Obukhov length scale, L, defined as

$$Ri_f = \frac{-\beta F_z}{\tau S}, \tag{4}$$

$$L = \frac{\tau^{3/2}}{-\beta F_z}, \tag{5}$$

where F_z is the vertical turbulent flux of potential temperature, and τ is the modulus of the vertical turbulent flux of momentum, Eq. 3 yields the following asymptotic relation

$$Ri_f = \frac{\tau^{1/2}}{SL} \to Ri_f^{\infty} \text{ at } Ri \to \infty, \tag{6}$$

where Ri_f^{∞} is the maximal flux Richardson number. In the EFB closure, Ri_f^{∞} is a universal constant ($Ri_f^{\infty} < 1$) to be determined empirically. The model reveals a transitional interval, $0.1 < Ri < 1$, separating the two turbulent regimes of essentially different nature: strong turbulence at $Ri << 1$ and weak turbulence that transports momentum but is much less efficient in transporting heat at $Ri > 1$.

Alternative new closure models with no *Ri*-critical also employ the TTE-budget equation but avoid the direct use of the budget equations for turbulent fluxes suggested by Mauritsen et al. (2007), and modification of their prior second-order turbulence closure by Canuto et al. (2008). L'vov et al. (2008) and L'vov and Rudenko (2008) have performed detailed analyses of the budget equations for the Reynolds stresses in the turbulent boundary layer (relevant to the strong turbulence regime) taking into consideration the dissipative effect of the horizontal heat flux explicitly, in contrast to the Zilitinkevich et al. (2007) "effective-dissipation approximation". All three budget equations for TKE, TPE and TTE were considered earlier by Canuto and Minotti (1993), Elperin et al. (2002) and Cheng et al. (2002). The third-order vertical transports of TKE and TPE caused by IGW in the two-layer system, comprising the turbulence-dominated atmospheric boundary layer and the IGW-dominated free atmosphere, was included in a simple turbulence closure model by Zilitinkevich (2002).

2 Large-Scale IGW in Stably Stratified Sheared Flows

In the present study we focus on the effect of large-scale IGW on stably stratified turbulence and do not discuss small-scale IGW. Accordingly, we consider the IGW wavelength/periods much larger than the turbulence spatial/time scales. This allows us to treat the large-scale IGW with respect to turbulence as a kind of mean flow with random phases, and to neglect molecular dissipation of IGW. We also neglect the feedback effect of turbulence on IGW. At the low frequency part of the IGW spectra, we limit our analysis to frequencies essentially exceeding the Coriolis frequency, so that the IGW under consideration are not affected by the Coriolis parameter, $f = 2\Omega \sin\varphi$, where Ω_i is the Earth's rotation vector parallel to the polar axis ($|\Omega_i| \equiv \Omega = 0.76 \times 10^{-4}\,\mathrm{s}^{-1}$), and φ is the latitude.

The large-scale IGW are characterized by the wave-field velocity, $\mathbf{V}^W = \left(V_1^W, V_2^W, V_3^W\right)$, and potential temperature, Θ^W, which satisfy the following equations (in the Boussinesq approximation for incompressible fluid):

$$\frac{\partial \mathbf{V}^W}{\partial t} = -\left(\mathbf{U}\cdot\nabla\right)\mathbf{V}^W - \nabla\left(\frac{P^W}{\rho_0}\right) + \beta\Theta^W\mathbf{e} - \left(\mathbf{V}^W\cdot\nabla\right)\mathbf{V}^W, \tag{7}$$

$$\frac{\partial \Theta^W}{\partial t} = -\left(\mathbf{U}\cdot\nabla\right)\Theta^W - \frac{1}{\beta}\left(\mathbf{V}^W\cdot\mathbf{e}\right)N^2 - \left(\mathbf{V}^W\cdot\nabla\right)\Theta^W, \tag{8}$$

and the conditions of incompressibility: $\mathrm{div}\,\mathbf{V}^W = 0$ and $\mathrm{div}\,\mathbf{U} = 0$. Here, $\mathbf{U}$ is the mean flow velocity, $\beta = g/T_0$ is the buoyancy parameter, $g = 9.81\,\mathrm{m\,s}^{-1}$ is the acceleration due to gravity, P^W is the pressure caused by IGW, $\mathbf{e}$ is the vertical unit vector, ρ_0 is the density of fluid, N is the Brunt–Väisälä frequency: $N^2 = \beta\partial\Theta/\partial z$, Θ is the potential temperature defined as $\Theta = T(P_0/P)^{1-1/\gamma}$, T is the absolute temperature, T_0 is its reference value, P is the pressure, P_0 is its reference value, and $\gamma = c_p/c_v = 1.41$ is the ratio of the specific heats. We do not consider nonlinear wave–wave interactions. Consequently, we neglect in Eqs. 7 and 8 the nonlinear terms $\left(\mathbf{V}^W\cdot\nabla\right)\mathbf{V}^W$ and $\left(\mathbf{V}^W\cdot\nabla\right)\Theta^W$, and apply to Eq. 7 the 'curl' operator to exclude the pressure (P^W) term. The solution of the linearised equations (7) and (8) in Fourier space reads:

$$V_\alpha^W = -\frac{k_\alpha k_z}{k_h^2}V_0^W(\mathbf{k})\cos(\omega t - \mathbf{k}\cdot\mathbf{r}), \tag{9}$$

for $\alpha = 1, 2$,

$$V_3^W \equiv V_z^W = V_0^W(\mathbf{k})\cos(\omega t - \mathbf{k}\cdot\mathbf{r}), \tag{10}$$

$$\Theta^W = -\frac{Nk}{\beta k_h}V_0^W(\mathbf{k})\sin(\omega t - \mathbf{k}\cdot\mathbf{r}) \tag{11}$$

(see, e.g., Turner 1973; Miropolsky 1981; Nappo 2002). Here, $\mathbf{k}$ is the wave vector; $k_\alpha = (k_x, k_y)$ is the horizontal wave vector, so that $k_h = \pm\sqrt{k_x^2 + k_y^2}$; and ω is the frequency of IGW:

$$\omega = \frac{k_h}{k}N + \mathbf{k}\cdot\mathbf{U}, \tag{12}$$

where $k = \sqrt{k_z^2 + k_h^2}$ is the total wavenumber. The second term in Eq. 12 is caused by the Doppler shift due to the sheared mean wind velocity $\mathbf{U}(z)$. Equations 9–10 satisfy the condition of incompressibility of the wave velocity field.

Propagation of IGW in a stably stratified sheared flow in the approximation of geometrical optics is determined by the following equations in the Hamiltonian form:

$$\frac{\partial \mathbf{r}}{\partial t} = \frac{\partial \omega}{\partial \mathbf{k}}, \tag{13}$$

$$\frac{\partial \mathbf{k}}{\partial t} = -\frac{\partial \omega}{\partial \mathbf{r}}, \tag{14}$$

where $\mathbf{r}$ is the radius vector of the centre of the wave packet, and $\mathbf{k}$ is the characteristic wave vector (see, e.g., Weinberg 1962). Since the Brunt–Väisälä frequency $N(z)$ and the mean velocity $\mathbf{U}(z)$ are functions only of the vertical coordinate, z, i.e., the only non-zero spatial derivative in Eq. 14 is $\partial\omega/\partial z$, Eqs. 12 and 14 yield $\mathbf{k}_h$ =constant. For the Hamiltonian system of Eqs. 13–14, $d\omega/dt = 0$, and Eq. 12 yields

$$\frac{k_h}{k(z)} N(z) + \mathbf{k} \cdot (\mathbf{U}(z) - \mathbf{U}(Z_0)) = \frac{k_h}{k_0} N(Z_0), \tag{15}$$

where Z_0 is the height of the IGW source, $k_0 = k(z = Z_0)$, and $\mathbf{k}_h(z) = \mathbf{k}_h(Z_0)$. We assume that the only source of the IGW is localised at $z = Z_0$ and neglect the generation and dissipation of waves during their propagation in the atmosphere.

Equation 15 determining the z-dependence of $k(z) = \sqrt{k_z^2(z) + k_h^2}$ implies that the IGW vertical wavenumbers, $k_z(z)$, change when the IGW propagate through the stably stratified sheared flow. For $Z_0 = 0$ (the IGW source is located at the surface), $k_z(z) = \sqrt{k^2(z) - k_h^2}$, and for $Z_0 = H$ (the IGW source is located at the upper boundary of the layer under consideration), $k_z(z) = -\sqrt{k^2(z) - k_h^2}$.

The IGW kinetic energy,

$$E_W \equiv \frac{1}{2} \int \left\langle \mathbf{V}_W^2(\mathbf{k}) \right\rangle_W d\,\mathbf{k} = \frac{1}{4} \int [V_0^W(\mathbf{k})]^2 d\,\mathbf{k}, \tag{16}$$

is related to the energy spectrum $e_W(\mathbf{k})$ of the ensemble of IGW: $E_W = \int [e_W(\mathbf{k})/2\pi k^2] d\mathbf{k}$, and $\langle \ldots \rangle_W$ denotes time average over a IGW period. Here, integration in $\mathbf{k}$ space over the angle θ between the axis z and the vector $\mathbf{k}$ is performed:

- from 0 to $\pi/2$ when the IGW source is located at the surface, and
- from $-\pi/2$ to 0, when the IGW source is located at the upper boundary of the layer.

Equations 9, 10 and 16 yield the expression for the wave amplitude: $[V_0^W(\mathbf{k})]^2 = (2k_h^2/\pi k^4) e_W(\mathbf{k})$. We assume that the energy spectrum of the ensemble of IGW generated at the point Z_0 is isotropic and has the power-law form:

$$e_W(k_0) = (\mu - 1) E_W H^{-(\mu+1)} k_0^{-\mu}, \tag{17}$$

where $E_W = \int [e_W(\mathbf{k}_0)/2\pi k_0^2] d\mathbf{k}_0 = \int e_W(k_0) dk_0$. Observations give different values of the exponent μ from 1 to 4 (Fofonoff 1969; Pochapsky 1972; Garrett and Munk 1979; Miropolsky 1981; Nappo 2002; Fritts and Alexander 2003). The wave vector k_0 varies from H^{-1} to L_W^{-1}, where L_W is the minimal wave length of the large-scale IGW. It is assumed that L_W is much larger than the turbulence length scale but much smaller than the depth of fluid, H.

For simplicity we consider the power-law form, Eq. 17, of the energy spectrum of the ensemble of IGW. This standard assumption is supported by many experiments (e.g., Nappo 2002; Fritts and Alexander 2003; and references therein). Other forms of the energy

spectrum would cause only minor changes in coefficients in the theoretical dependencies obtained below (in Sects. 4–6) but would not change their form. The exponent μ is a free parameter, which must exceed unity and be less than 4 (see Nappo 2002; Fritts and Alexander 2003; and references therein). Variations in μ change only the coefficient on the r.h.s. of Eq. 43 for the IGW transport of momentum (see Sect. 4), and only weakly affect other theoretical dependencies.

3 Basic Equations for Turbulent Flows Accounting for Large-Scale IGW

We consider the large-scale IGW whose periods and wavelengths are much larger than the turbulent time and length scales. Therefore, although the IGW have random phases, the wave field interacts with small-scale turbulence in same way as the mean flow. We represent the total velocity as the sum of the mean-flow velocity,$\mathbf{U}(z)$, the wave-field velocity, $\mathbf{V}^W$, and the turbulent velocity, $\mathbf{u}$, and neglect the wave–wave interactions at large scales but take into account the turbulence–wave interactions. We limit our analysis to flows in which the vertical variations [along the x_3 (or z) axis] of the mean wind velocity $\mathbf{U} = (U_1, U_2, U_3)$ and potential temperature Θ are much larger than the horizontal variations [along x_1, x_2 (or x, y) axes], so that the terms associated with the horizontal gradients in the budget equations for turbulent statistics can be neglected.

For typical atmospheric flows, the vertical scales (limited to the height scale of the atmosphere or the ocean: $H \sim 10^4$ m) are much smaller than the horizontal scales, so that the mean vertical velocity is much smaller than the horizontal velocity. To close the Reynolds equations in these conditions, we need only the vertical component, F_z, of the potential temperature flux and the two components of the vertical turbulent flux of momentum that comprise the turbulent contributions, τ_{13} and τ_{23}, and the direct contributions of the large-scale IGW, τ_{1j}^{WW} and τ_{2j}^{WW}.

The mean-flow momentum equations and thermodynamic energy equation accounting for the large-scale IGW can be written as follows:

$$\frac{DU_1}{Dt} = fU_2 - \frac{1}{\rho_0}\frac{\partial P}{\partial x} - \frac{\partial \tau_{13}}{\partial z} - \frac{\partial \tau_{1j}^{WW}}{\partial x_j}, \tag{18}$$

$$\frac{DU_2}{Dt} = -fU_1 - \frac{1}{\rho_0}\frac{\partial P}{\partial y} - \frac{\partial \tau_{23}}{\partial z} - \frac{\partial \tau_{2j}^{WW}}{\partial x_j}, \tag{19}$$

$$\frac{D\Theta}{Dt} = -\frac{\partial F_z}{\partial z} - \frac{\partial F_j^{WW}}{\partial x_j} + J, \tag{20}$$

where $D/Dt = \partial/\partial t + U_k \partial/\partial x_k$; $\tau_{ij} = \langle u_i u_j \rangle$; $F_i = \langle u_i\, \theta \rangle$; t is the time; ρ_0 is the mean density; J is the heating/cooling rate ($J = 0$ in adiabatic processes); P is the mean pressure; $\mathbf{u} = (u_1, u_2, u_3) = (u, \mathrm{v}, \mathrm{w})$ and θ are the velocity and potential-temperature fluctuations, respectively. The angle brackets $\langle \ldots \rangle$ denote the ensemble average over turbulent fluctuations. Besides the ensemble averaging, Eqs. 18–20 are averaged in time over the IGW period. This procedure is denoted by $\langle \ldots \rangle_W$. It implies that $\langle \cos(\omega t - \mathbf{k}\cdot\mathbf{r}) \rangle_W = \langle \sin(\omega t - \mathbf{k}\cdot\mathbf{r}) \rangle_W = 0$ and $\langle \cos^2(\omega t - \mathbf{k}\cdot\mathbf{r}) \rangle_W = 1/2$.

Any direct effects of IGW on the mean flow are determined by the second-order moments

$$\tau_{\alpha j}^{WW} = \left\langle V_\alpha^W V_j^W \right\rangle_W, \quad \alpha = 1, 2, \tag{21a}$$

$$F_j^{WW} = \left\langle V_j^W \, \Theta^W \right\rangle_W, \tag{21b}$$

which determine the wave-induced fluxes of momentum and potential temperature. In the linear theory, IGW do not transfer heat (so that $F_j^{WW} = 0$) but transfer momentum (e.g., Nappo 2002). Accordingly, we neglect F_j^{WW} but account for $\tau_{\alpha j}^{WW}$ (see Sect. 4.2).

The budget equations for the turbulent kinetic energy (TKE), $E_K = \frac{1}{2}\langle u_i u_i \rangle$, the squared potential temperature fluctuations, $E_\theta = \frac{1}{2}\langle \theta^2 \rangle$, and the potential-temperature flux, $F_i = \langle u_i \, \theta \rangle$, accounting for large-scale IGW can be written as follows:

$$\frac{DE_K}{Dt} + \frac{\partial \Phi_K}{\partial z} = -\tau_{i3}\frac{\partial U_i}{\partial z} + \beta F_z - \varepsilon_K - \left\langle \tau_{ij}^W \frac{\partial V_i^W}{\partial x_j} \right\rangle_W + \beta \left\langle V_z^W \, \Theta^W \right\rangle_W, \tag{22}$$

$$\frac{DE_\theta}{Dt} + \frac{\partial \Phi_\theta}{\partial z} = -F_z \frac{\partial \Theta}{\partial z} - \varepsilon_\theta - \left\langle F_j^W \frac{\partial \Theta^W}{\partial x_j} \right\rangle_W, \tag{23}$$

$$\frac{DF_i}{Dt} + \frac{\partial}{\partial x_j}\Phi_{ij}^{(F)} = \beta_i \langle \theta^2 \rangle + \frac{1}{\rho_0}\langle \theta \nabla_i p \rangle - \tau_{i3}\frac{\partial \Theta}{\partial z} - F_j \frac{\partial U_i}{\partial x_j} - \varepsilon_i^{(F)} - \left\langle \tau_{ij}^W \frac{\partial \Theta^W}{\partial x_j} \right\rangle_W - \left\langle F_j^W \frac{\partial V_i^W}{\partial x_j} \right\rangle_W. \tag{24}$$

Recall that E_θ is proportional to the turbulent potential energy (TPE):

$$E_P = \frac{\beta^2}{N^2} E_\theta, \tag{25}$$

so that Eq. 23 is equivalent to the budget equation for E_P.

As already mentioned, we are interested, first of all, in the vertical flux, $F_3 = F_z = \langle \mathrm{w}\theta \rangle$, whose budget equation is

$$\frac{DF_z}{Dt} + \frac{\partial}{\partial z}\Phi_F = \beta \langle \theta^2 \rangle + \frac{1}{\rho_0}\left\langle \theta \frac{\partial}{\partial z} p \right\rangle - \langle \mathrm{w}^2 \rangle \frac{\partial \Theta}{\partial z} - \varepsilon_z^{(F)} - \left\langle \tau_{j3}^W \frac{\partial \Theta^W}{\partial x_j} \right\rangle_W - \left\langle F_j^W \frac{\partial V_z^W}{\partial x_j} \right\rangle_W. \tag{26}$$

Accounting for IGW, the budget equation for the Reynolds stresses, $\tau_{ij} = \langle u_i u_j \rangle$, reads:

$$\frac{D\tau_{ij}}{Dt} + \frac{\partial}{\partial x_k}\Phi_{ijk}^{(\tau)} = -\tau_{ik}\frac{\partial U_j}{\partial x_k} - \tau_{jk}\frac{\partial U_i}{\partial x_k} + \beta(F_j\delta_{i3} + F_i\delta_{j3}) + Q_{ij} - \varepsilon_{ij}^{(\tau)} - \left\langle \tau_{ik}^W \frac{\partial V_j^W}{\partial x_k} \right\rangle_W - \left\langle \tau_{jk}^W \frac{\partial V_i^W}{\partial x_k} \right\rangle_W. \tag{27}$$

Hence, the budget equations for the non-diagonal, $\tau_{\alpha 3}$, and diagonal, $\tau_{\alpha\alpha} = 2E_\alpha$, components of the Reynolds stresses, $\tau_{ij} = \langle u_i u_j \rangle$, can be written as follows:

$$\frac{D\tau_{\alpha 3}}{Dt} + \frac{\partial}{\partial z}\Phi_{\alpha}^{(\tau)} = -\left\langle \mathrm{w}^2 \right\rangle \frac{\partial U_{\alpha}}{\partial z} + \beta F_{\alpha} + Q_{\alpha 3} - \varepsilon_{\alpha 3}^{(\tau)} - \left\langle \tau_{\alpha j}^{W} \frac{\partial V_z^{W}}{\partial x_j} \right\rangle_W - \left\langle \tau_{j3}^{W} \frac{\partial V_{\alpha}^{W}}{\partial x_j} \right\rangle_W, \tag{28}$$

$$\frac{DE_{\alpha}}{Dt} + \frac{\partial}{\partial z}\Phi_{\alpha}^{(\tau)} = -\tau_{\alpha 3}\frac{\partial U_{\alpha}}{\partial z} + \frac{1}{2}Q_{\alpha\alpha} - \varepsilon_{\alpha\alpha}^{(\tau)} - \left\langle \tau_{\alpha j}^{W} \frac{\partial V_{\alpha}^{W}}{\partial x_j} \right\rangle_W, \tag{29}$$

$$\frac{DE_z}{Dt} + \frac{\partial}{\partial z}\Phi_{z}^{(\tau)} = \beta F_z + \frac{1}{2}Q_{33} - \varepsilon_{33}^{(\tau)} - \left\langle \tau_{j3}^{W} \frac{\partial V_z^{W}}{\partial x_j} \right\rangle_W, \tag{30}$$

where $\beta_i = \beta e_i$; $\mathbf{e} = (e_1,\ e_2,\ e_3)$ is the vertical unit vector; $\tau_{\alpha 3} = \langle u_{\alpha}\mathrm{w}\rangle$ ($\alpha = 1,\ 2$) are the two components of the vertical turbulent flux of momentum, and $F_{\alpha} = \langle u_{\alpha}\theta\rangle$ are the horizontal fluxes of potential temperature ($\alpha = 1,\ 2$). In Eq. 29 we do not apply the summation convention for the double Greek indices.

The terms Φ_K, Φ_{θ} in Eqs. 22–23 are the third-order moments determining turbulent fluxes of E_K and E_{θ}:

$$\mathbf{\Phi}_K = \frac{1}{\rho_0}\langle p\ \mathbf{u}\rangle + \frac{1}{2}\left\langle u^2\ \mathbf{u}\right\rangle + \mathbf{\Phi}_K^{W}, \tag{31a}$$

whose z-component is

$$\Phi_K = \frac{1}{\rho_0}\langle p\ \mathrm{w}\rangle + \frac{1}{2}\left\langle \mathbf{u}^2\ \mathrm{w}\right\rangle + \Phi_K^{W}, \tag{31b}$$

$$\mathbf{\Phi}_{\theta} = \frac{1}{2}\left\langle \theta^2\ \mathbf{u}\right\rangle + \mathbf{\Phi}_{\theta}^{W}, \tag{31c}$$

whose z-component is

$$\Phi_{\theta} = \frac{1}{2}\left\langle \theta^2\ \mathrm{w}\right\rangle + \Phi_{\theta}^{W}, \tag{31d}$$

where the terms marked with the superscript "W" denote the wave-driven turbulent fluxes of E_K and E_{θ}.

The terms $\Phi_{ij}^{(F)}$, $\Phi_F = \Phi_{33}^{(F)}$, $\Phi_{ijk}^{(\tau)}$ and $\Phi_{\alpha}^{(\tau)}$in Eqs. 24–30 are the third-order moments representing the fluxes of fluxes:

$$\Phi_{ij}^{(F)} = \frac{1}{2\rho_0}\langle p\ \theta\rangle\ \delta_{ij} + \left\langle u_i u_j \theta\right\rangle + \Phi_{ij}^{(FW)}, \tag{32a}$$

$$\Phi_{33}^{(F)} = \Phi_{\mathrm{F}} = \frac{1}{2\rho_0}\langle p\ \theta\rangle + \left\langle \mathrm{w}^2\theta\right\rangle + \Phi_{33}^{(FW)}, \tag{32b}$$

$$\Phi_{ijk}^{(\tau)} = \left\langle u_i u_j u_k\right\rangle + \frac{1}{\rho_0}\left(\langle p u_i\rangle\ \delta_{jk} + \left\langle p u_j\right\rangle \delta_{ik}\right) + \Phi_{ijk}^{(\tau W)}, \tag{33a}$$

$$\Phi_{i}^{(\tau)} = \Phi_{i33}^{(\tau)} = \left\langle u_i \mathrm{w}^2\right\rangle + \frac{1}{\rho_0}\langle p u_i\rangle + \Phi_{i}^{(\tau W)}, \tag{33b}$$

where the terms marked with the superscript "(W)" denote the wave-driven turbulent fluxes of fluxes, and Q_{ij} are correlations between the fluctuations of the pressure, p, and the velocity shears:

$$Q_{ij} = \frac{1}{\rho_0}\left\langle p\left(\frac{\partial u_i}{\partial x_j} + \frac{\partial u_j}{\partial x_i}\right)\right\rangle. \tag{34}$$

The terms, $\varepsilon_k, \varepsilon_{ij}^{(\tau)}$, ε_θ and $\varepsilon_i^{(F)}$ are determined by the following relations,

$$\varepsilon_K = \nu \left\langle \frac{\partial u_i}{\partial x_k} \frac{\partial u_i}{\partial x_k} \right\rangle, \tag{35a}$$

$$\varepsilon_{ij}^{(\tau)} = 2\nu \left\langle \frac{\partial u_i}{\partial x_k} \frac{\partial u_j}{\partial x_k} \right\rangle, \tag{35b}$$

$$\varepsilon_\theta = -\kappa \left\langle \theta \, \Delta \, \theta \right\rangle, \tag{36a}$$

$$\varepsilon_i^{(F)} = -\kappa \left(\left\langle u_i \, \Delta \, \theta \right\rangle + \mathrm{Pr} \left\langle \theta \, \Delta \, u_i \right\rangle \right), \tag{36b}$$

where ν is the kinematic viscosity, κ is the temperature diffusivity, and $Pr = \nu/\kappa$ is the Prandtl number.

The diagonal terms, $\varepsilon_{11}^{(\tau)}$, $\varepsilon_{22}^{(\tau)}$, $\varepsilon_{33}^{(\tau)}$, ε_K (the sum of $\varepsilon_{ii}^{(\tau)}$), ε_θ, $and \varepsilon_i^{(F)}$, representing the dissipation rates for $\tau_{\alpha\alpha}$, E_K, E_θ and $F_i^{(F)}$, respectively, are expressed using the Kolmogorov (1941) hypothesis:

$$\varepsilon_K = \frac{E_K}{C_K \, t_T}, \tag{37a}$$

$$\varepsilon_{\alpha\alpha}^{(\tau)} = \frac{\tau_{\alpha\alpha}}{C_K \, t_T}, \tag{37b}$$

$$\varepsilon_\theta = \frac{E_\theta}{C_P \, t_T}, \tag{37c}$$

$$\varepsilon_i^{(F)} = \frac{F_i}{C_F \, t_T}, \tag{37d}$$

where t_T is the turbulent dissipation time scale, C_K, C_P and C_F are dimensionless constants, and the summation convention is not applied to the double Greek indices.

In the budget equations for the vertical turbulent fluxes of momentum, $\tau_{\alpha 3}$ ($\alpha = 1, 2$), the terms $\varepsilon_{\alpha 3}^{(\tau)}$ dependent on the molecular viscosity are usually small, whereas the contributions of the terms βF_α and $Q_{\alpha 3}$ to dissipation are overwhelming. Following Zilitinkevich et al. (2007), we introduce the Reynolds-stress "effective dissipation rates":

$$\varepsilon_{\alpha 3(\mathrm{eff})} \equiv \varepsilon_{\alpha 3}^{(\tau)} - \beta F_\alpha - Q_{\alpha 3}, \tag{38}$$

for $\alpha = 1, 2$, and, by analogy with Eq. 37, apply to them the closure hypothesis:

$$\varepsilon_{\alpha 3(\mathrm{eff})} = \frac{\tau_{\alpha 3}}{t_\tau} = \frac{\tau_{\alpha 3}}{C_\tau \, t_T}, \tag{39}$$

where t_τ is the effective dissipation time scale, and C_τ is a dimensionless coefficient accounting for the difference between t_τ and t_T. The turbulent dissipation time scale, t_T, is expressed through the vertical turbulent length scale, l_z, and the kinetic energy of the vertical velocity fluctuations:

$$t_T = \frac{l_z}{E_z^{1/2}}. \tag{40}$$

Equations 18–20 and 22–30 are obtained by averaging over the ensemble of turbulent fluctuations and over the period of large-scale IGW. These equations in a general form without the IGW terms can be found, e.g., in Kaimal and Fennigan (1994), Kurbatsky (2000),

Cheng et al. (2002) and Canuto and Minotti (1993). Equation 22 is presented in Einaudi and Finnigan (1993). Hereafter we restrict our analysis to the effects of IGW on the second-order statistics and leave the IGW third-order moments (the fluxes of energies and the fluxes of momentum and heat fluxes) for further study.

The IGW terms in the above equations include the wave-field velocity and temperature, V_i^W and Θ^W, specified by Eqs. 9–11; and the instantaneous Reynolds stresses, τ_{ij}^W, and turbulent flux of potential temperature, F_i^W, caused by the IGW–turbulence interaction. We determine τ_{ij}^W approximately—subtracting Eq. 27 from the ensemble-averaged equation for τ_{ij} but not averaged over the IGW period, assuming that $\omega t_T \ll 1$ and $\varepsilon_i^{(\tau)} = \tau_{ij}^W/(C_\tau t_T)$, and omitting the terms quadratic in wave amplitude, which do not contribute to the correlations $\left\langle \tau_{ij}^W \left(\partial V_i^W/\partial x_j\right)\right\rangle_W$ and $\left\langle \tau_{ij}^W \left(\partial \Theta^W/\partial x_j\right)\right\rangle_W$:

$$\tau_{ij}^W \approx -C_\tau t_T \left(\tau_{ik} \frac{\partial V_j^W}{\partial x_k} + \tau_{jk} \frac{\partial V_i^W}{\partial x_k} \right). \tag{41}$$

Similarly, we determine F_i^W also approximately—subtracting Eq. 24 from the ensemble-averaged equation for F_i but not averaged over the IGW period, assuming that $\omega t_T \ll 1$ and $\varepsilon_i^{(F)} = F_i^W/(C_F t_T)$, and omitting the terms quadratic in wave amplitude, which do not contribute to the correlations $\left\langle F_j^W \left(\partial V_i^W/\partial x_j\right)\right\rangle_W$ and $\left\langle F_j^W \left(\partial \Theta^W/\partial x_j\right)\right\rangle_W$:

$$F_i^W \approx -C_F t_T \left(\tau_{ij} \frac{\partial \Theta^W}{\partial x_j} + \tau_{i3}^W \frac{\partial \Theta}{\partial z} + F_j \frac{\partial V_i^W}{\partial x_j} \right). \tag{42}$$

Concrete effects of IGW on turbulence are considered in the following sections.

4 The Effects of Large-Scale IGW on the Turbulent Transports and Energies

4.1 The IGW Transport of Momentum

For simplicity, we consider the stationary, homogeneous regime of turbulence, neglect the effect of the Earths rotation, and assume that the mean wind velocity is directed along the x-axis: $\mathbf{U} = (U,\ 0,\ 0)$. Using Eqs. 9 and 10 for the IGW velocity field, Eq. 17 for the IGW energy spectrum, and assuming that $|U(z) - U(Z_0)| \ll L_W N(Z_0)$, integration over the spectrum of the IGW vertical flux of momentum, $\tau_{\alpha 3}^{WW}(\mathbf{k}_0) = -k_\alpha k_z(k_0) e_W(k_0)/[\pi k_0^2 k^2(k_0)]$, in $\mathbf{k}$-space yields:

$$\begin{aligned} \tau_{\alpha 3}^{WW} &= \left\langle V_\alpha^W V_z^W \right\rangle_W = \int \tau_{\alpha 3}^{WW}(\mathbf{k}_0)\, d\mathbf{k}_0 \\ &= \pm \frac{\Gamma[U(Z_0) - U(z)]}{3N(z)H} \left[(Q+4)\, E(Q) - (Q+2)\, K(Q) \right] E_W, \end{aligned} \tag{43}$$

where Q is the dimensionless lapse rate:

$$Q = \left[\frac{N(z)}{N(Z_0)} \right]^2. \tag{44}$$

The coefficient Γ is expressed through the exponent μ in the power-law energy spectrum of IGW, namely, for $1 < \mu < 2$:

$$\Gamma = \frac{\mu - 1}{2 - \mu} \left(\frac{H}{L_w} \right)^{2-\mu}, \tag{45a}$$

for $\mu = 2$:

$$\Gamma = \ln \left(\frac{H}{L_W} \right), \tag{45b}$$

for $2 < \mu$:

$$\Gamma = \frac{\mu - 1}{\mu - 2}, \tag{45c}$$

where $K(Q) = \int_0^{\pi/2} (1 - Q^{-1} \sin^2 \theta)^{-1/2} d\theta$ and $E(Q) = \int_0^{\pi/2} (1 - Q^{-1} \sin^2 \theta)^{1/2} d\theta$ are the complete elliptic integrals of the first and the second types, respectively. Plus or minus signs in Eq. 43 correspond to the cases when the IGW sources are located at the lower ($Z_0 = 0$) or upper ($Z_0 = H$) boundaries, respectively. The condition, $|U(z) - U(Z_0)| \ll L_W N(Z_0)$, is introduced to simplify further derivations and results, which otherwise become too cumbersome. This assumption is not principal and can be relaxed. At large Q, the integrals are $K(Q) = E(Q) \approx \pi/2$ and Eq. 43 reads:

$$\tau_{\alpha 3}^{WW} \approx \pm \frac{\pi}{3} \frac{\Gamma[U(z) - U(Z_0)]}{N(z) H} E_W. \tag{46}$$

When the IGW sources are located at the lower boundary ($Z_0 = 0$) and IGW are generated by the interaction of the flow with mountains or hills, $\tau_{\alpha 3}^{WW}$ is negative so that IGW transport momentum downward and increase the total downward momentum flux, $\tau_{\alpha 3} + \tau_{\alpha 3}^{WW}$ (where $\tau_{\alpha 3}^{WW} < 0$ and $\tau_{\alpha 3} < 0$). This well-known mechanism is called "wave drag" (e.g., Nappo 2002). When the IGW sources are located at the upper boundary ($Z_0 = H$), e.g., when IGW propagating in the free atmosphere are trapped by the stably stratified atmospheric boundary layer (ABL), IGW transport momentum upwards ($\tau_{\alpha 3}^{WW} > 0$) because $U(z) < U(Z_0)$. Then the vertical flux of the momentum $\tau_{\alpha 3}^{WW}$ is subtracted from the turbulent flux, $\tau_{\alpha 3} < 0$, and the total vertical flux of momentum reduces. These effects can be parameterized using Eq. 43.

4.2 The IGW Production of Turbulent Energies and Turbulent Flux of Potential Temperature

The IGW contribution to the production of TKE, E_K, is

$$\Pi^W = -\left\langle \tau_{ij}^W \frac{\partial V_i^W}{\partial x_j} \right\rangle_W = \int \Pi^W(\mathbf{k}_0)\, d\mathbf{k}_0, \tag{47}$$

where $\Pi^W(\mathbf{k}_0)$ is the production of E_K in $\mathbf{k}$-space, caused by the diagonal components of the tensor τ_{jk}:

$$\Pi^W(\mathbf{k}_0) = C_\tau t_T \tau_{jk} k_j k_k \frac{e_W(k_0)}{\pi k_0^2} = 2 C_\tau t_T \left(E_z k_z^2(k_0) + E_x k_x^2 + E_y k_y^2 \right) \frac{e_W(k_0)}{\pi k_0^2}. \tag{48}$$

Integration over $\mathbf{k}$ yields

$$\Pi^W = \frac{4 C_\tau}{3} E_z^{1/2} l_z S^2 G \left[\frac{1}{A_z} + 3(Q - 1) \right], \tag{49}$$

where $A_z = E_z/E_K$ is ratio of the vertical kinetic energy to TKE, G is a dimensionless "wave-energy parameter" proportional to the normalized IGW kinetic energy, E_W:

$$G = \frac{E_W}{S^2H^2}\frac{\mu-1}{3-\mu}\left(\frac{H}{L_W}\right)^{3-\mu}. \tag{50}$$

In further analysis we assume that the wavelengths are much shorter than the basic depth scale: $L_w \ll H$.

The IGW contribution to the production of the vertical component of TKE, E_z, is

$$\Pi_z^w = -\left\langle \tau_{j3}^W \frac{\partial V_z^W}{\partial x_j}\right\rangle_W = \int \Pi_z^W(\mathbf{k}_0)\, d\mathbf{k}_0, \tag{51}$$

where $\Pi_z^W(\mathbf{k}_0) = \Pi^W(\mathbf{k}_0)k_h^2/k^2$ is the production of E_z in $\mathbf{k}$-space. Integration over $\mathbf{k}$ in Eq. 51 yields

$$\Pi_z^W = \frac{8C_\tau}{3}E_z^{1/2}l_zS^2G\left[1+\frac{2}{5Q}(A_z^{-1}-3)\right]. \tag{52}$$

The IGW contribution to the productions of the longitudinal, E_x, and the transverse, E_x, components of TKE are

$$\Pi_x^W = \Pi_y^W = \frac{1}{2}\left(\Pi^W - \Pi_z^W\right) = \frac{2C_\tau}{3}E_z^{1/2}l_zS^2G\left[3Q-2+(A_z^{-1}-3)\left(1-\frac{4}{5Q}\right)\right]. \tag{53}$$

The IGW contribution to the production of $E_\theta = \frac{1}{2}\langle\theta^2\rangle$ is

$$\Pi_\theta^W = -\left\langle F_j^W \frac{\partial\Theta^W}{\partial x_j}\right\rangle_W = \int \Pi_\theta^W(\mathbf{k}_0)\, d\mathbf{k}_0, \tag{54}$$

where

$$\Pi_\theta^W(\mathbf{k}_0) = 2C_F t_T \frac{N^2(z)}{\beta^2}\left(E_z k_z^2(k_0) + E_x k_x^2 + E_y k_y^2\right)\frac{e_W(k_0)}{\pi k_0^2}, \tag{55}$$

and C_F is an empirical dimensionless constant. Here, we take into account that only diagonal components of the tensor τ_{jk} contribute to $\Pi_\theta^W(\mathbf{k}_0)$ (similarly to the production of E_K). Integration in Eq. 54 in $\mathbf{k}$-space yields

$$\Pi_\theta^W = F_\theta^W \frac{N^2(z)}{\beta}, \tag{56}$$

where F_θ^W is the wave-induced turbulent flux of potential temperature:

$$F_\theta^W = \frac{4C_F}{3\beta}E_z^{1/2}l_zS^2G\left[A_z^{-1}+3(Q-1)\right]. \tag{57}$$

Note that the vertical flux of potential temperature is negative (downward), which is the reason for the negative production (see Eq. 56). The IGW contribution to the production of E_θ is affected by F_θ^W, which in its turn is affected by E_θ.

In order to determine the direct effect of IGW on F_θ^W, we take into account that $\langle V_i\Theta^W\rangle_W = 0$, which yields $\left\langle \tau_{ij}^W \frac{\partial\Theta^W}{\partial x_j}\right\rangle_W = 0$. Then, using Eq. 52, the term $\left\langle F_j^W\left(\partial V_z^W/\partial x_j\right)\right\rangle_W$ describing the production of F_z in Eq. 26, can be written as follows:

$$\Pi_F^W = -\left\langle F_j^W \frac{\partial V_z^W}{\partial x_j} \right\rangle_W = -C_F \Pi_{33}^W \frac{l_z}{E_z^{1/2}} \frac{N^2(z)}{\beta}$$
$$= -\frac{8C_F C_\tau}{3} l_z^2 S^2 G \left[1 + \frac{2}{5Q}(A_z^{-1} - 3)\right] \frac{N^2}{\beta}. \quad (58)$$

The production of the non-diagonal components of the Reynolds stresses, $\tau_{\alpha 3}$, caused by IGW is

$$\Pi_{\tau\alpha}^W = -\left\langle \tau_{\alpha j}^W \frac{\partial V_z^W}{\partial x_j} \right\rangle_W - \left\langle \tau_{j3}^W \frac{\partial V_\alpha^W}{\partial x_j} \right\rangle_W = \int \Pi_{\tau\alpha}^W(\mathbf{k}_0)\, d\mathbf{k}_0, \quad (59)$$

where

$$\Pi_{\tau\alpha}^W(\mathbf{k}_0) = -2C_\tau t_T \tau_{ij} \frac{k_i k_j k_\alpha k_z}{k^2(k_0)} \frac{e_W(k_0)}{\pi k_0^2}. \quad (60)$$

Here we take into account that only diagonal components of the tensor τ_{jk} contribute to $\Pi_{\tau\alpha}^W(\mathbf{k}_0)$. Using Eq. 17 and integrating in $\mathbf{k}$-space in Eq. 59 yields:

$$\Pi_{\tau\alpha}^W = -\frac{8C_\tau}{3} \tau_{\alpha 3} \frac{l_z S^2}{E_z^{1/2}} G \left(1 - \frac{4}{5Q}\right). \quad (61)$$

Finally, the production of the total turbulent energy (TTE) $E = E_K + E_P$ caused by IGW is

$$\Pi_E^W = \Pi^W + \Pi_\theta^W \frac{\beta^2}{N^2}. \quad (62)$$

Consequently, IGW contribute to the production of both TKE and TPE, in contrast to the mean shear, which contributes only to the TKE production.

5 Turbulence Closures with and without IGW for the Steady-State Regime

5.1 The Background Energy- and Flux-Budget (EFB) Closure Model

In this section we present a refined version of the EFB turbulence closure model (Zilitinkevich et al. 2007). The latter employed the same equations as Eqs. 22–30 but without the IGW terms (marked in the present paper with the superscript "W"). Zilitinkevich et al. (2007) assumed that the dissipation constants for the kinetic and potential energies were equal ($C_P = C_K$) and had to admit that the ratio $C_\tau = t_\tau / t_T$ depends on Ri. Our analysis of the experimental data revealed that this assumption was not quite correct:

- the dissipation constants are different: $C_P / C_K = 0.72$,
- accounting for this difference, the coefficient C_τ turns into a universal (independent of Ri) constant.

This leads to an essentially simplified EFB closure model—with $C_P \neq C_K$ but $C_\tau =$ constant, and yields a very simple formula for the eddy viscosity: $K_M = 2C_\tau E_z^{1/2} l_z$. Note that principally the same result, $K_M (E_z^{1/2} l_z)^{-1} =$ constant, has been derived from a quite rigorous analysis of the budget equations for the Reynolds stresses in $\mathbf{k}$-space based on the τ-approximation (Elperin et al. 2002, 2006).

In order to better fit the EFB model to the available observational data on the vertical anisotropy, Zilitinkevich et al. (2007) proposed a modified formulation of the Rotta (1951)

return-to-isotropy hypothesis. Considering the IGW–turbulence interaction, we now recognise that the apparent deviations from the Rotta hypothesis are caused by the effect of IGW. Therefore, it is only natural to retain the universally recognised classical formulation whereby the sum of the terms $\sum Q_{ii} = \sum \rho_0^{-1} \langle p \partial u_i / \partial x_i \rangle$ in Eqs. 28–30 is zero because of the continuity equation $\left(\sum \partial u_i / \partial x_i = 0\right)$, so that $Q_{\alpha\alpha}$ describe the energy transfer from the high energy to the lower energy components:

$$Q_{\alpha\alpha} = -\frac{2C_r}{3C_K t_T}(3E_\alpha - E_K), \tag{63}$$

where C_r is a dimensionless constant accounting for the difference between the relaxation (return to isotropy) and dissipation time scales.

The terms $\beta \langle \theta^2 \rangle$ and $\rho_0^{-1} \langle \theta \partial p / \partial z \rangle$ in the budget equation (26) for the vertical turbulent flux of potential temperature play a very important role. Zilitinkevich et al. (2007) showed that $\rho_0^{-1} \langle \theta \partial p / \partial z \rangle$ is negative and scales as $\beta \langle \theta^2 \rangle$, which yields:

$$\beta \langle \theta^2 \rangle + \rho_0^{-1} \langle \theta \partial p / \partial z \rangle = C_\theta \beta \langle \theta^2 \rangle, \tag{64}$$

where $C_\theta < 1$ is an empirical constant. We retain this approximation in the present study.

On these grounds we afford different values of C_P and C_K and essentially simplify the original EFB model setting $C_\tau =$ constant and using the standard return-to isotropy formulation, Eq. 63.

5.2 The EFB + IGW Closure Model

Now we generalise the refined EFB closure model (Sect. 5.1) considering the budget equations (22)–(30) with the IGW terms determined by Eqs. 49, 52, 56–58. To demonstrate the role of IGW, we compare the two versions of the closure—with and without IGW—*in the steady-state regime of turbulence*, when the left-hand sides (l.h.s.) of all budget equations are zero, so that the model reduces to a system of algebraic equations. We focus on the turbulent energies and fluxes and leave the problem of determining the vertical turbulent length scale, l_z, for a separate study. In further derivations we basically follow Zilitinkevich et al. (2007) but introduce the changes indicated in Sect. 5.1 and include the effects of IGW presented in Sects. 3 and 4.

In the steady state, the system of equations (22)–(23), (26), (28) and (30) reads:

$$-\tau_{i3}\frac{\partial U_i}{\partial z} + \beta F_z - \frac{E_K}{C_K\, t_T} + \Pi^W = 0, \tag{65}$$

$$-F_z\frac{N^2}{\beta} - \frac{E_\theta}{C_P\, t_T} + \Pi^W_\theta = 0, \tag{66}$$

$$2C_\theta \beta E_\theta - 2E_z\frac{N^2}{\beta} - \frac{F_z}{C_F\, t_T} + \Pi^W_F = 0, \tag{67}$$

$$-2E_z\frac{\partial U_\alpha}{\partial z} - \frac{\tau_{\alpha 3}}{C_\tau\, t_T} + \Pi^W_{\tau\alpha} = 0, \tag{68}$$

$$\beta F_z - \frac{C_r}{3C_K t_T}(3E_z - E_K) - \frac{E_z}{C_K\, t_T} + \Pi^W_z = 0, \tag{69}$$

where the productions, Π^W, Π^W_z Π^W_θ, Π^W_F and $\Pi^W_{\tau\alpha}$, are determined by Eqs. 49, 52, 56, 58 and 61.

In the steady state, Eqs. 65–69 specify the turbulent energies and the vertical turbulent fluxes as dependent on the turbulent length scale, l_z, and the following dimensionless external parameters:

- gradient Richardson number Ri, Eq. 1,
- wave-energy parameter G, Eq. 50,
- lapse rate parameter Q, Eq. 44, characterising the IGW refraction.

A remarkable feature of this system is that l_z drops out from the equations specifying the dimensionless parameters of turbulence,[1] so that the latter are determined as universal functions of Ri, G and Q, without any knowledge about l_z. In particular, for the dimensionless vertical TKE $\hat{E}_z$, the vertical flux of potential temperature $\hat{F}_z$ and the energy ratio A_z defined as

$$\hat{E}_z \equiv \frac{E_z}{(Sl_z)^2}, \tag{70a}$$

$$\hat{F}_z \equiv \frac{-\beta F_z}{E_z^{1/2} l_z S^2}, \tag{70b}$$

$$A_z \equiv \frac{E_z}{E_K}, \tag{70c}$$

the system reduces to the following three algebraic equations:

$$\hat{E}_z - \frac{2C_K C_r C_\tau}{3(1+C_r)}\left\{1 - \left(1+\frac{3}{C_r}\right)\frac{\hat{F}_z}{2C_\tau} + G\left[\frac{1}{3A_z}\left(1+\frac{12}{5C_r Q}\right) + Q - 1 + \frac{2}{C_r}\left(1-\frac{6}{5Q}\right)\right]\right\} = 0 \tag{71}$$

$$A_z - \frac{\hat{E}_z}{2C_K C_\tau}\left(1 - \frac{\hat{F}_z}{2C_\tau} + \frac{2G}{3}\left(A_z^{-1} + 3(Q-1)\right)\right)^{-1} = 0, \tag{72}$$

$$G\left[\frac{1}{A_z}\left(\frac{2C_\tau}{5Q} - C\right) + C_\tau\left(1-\frac{6}{5Q}\right) - 3C(Q-1)\right] + \frac{3\hat{E}_z}{4C_F}\left[1 - \hat{F}_z\left(\frac{1}{2C_F \mathrm{Ri}} + \frac{C_\theta C_P}{\hat{E}_z}\right)\right] = 0, \tag{73}$$

where $C = C_\theta C_K$. The system of algebraic equations (71)–(73) determines the three functions:

$$\hat{E}_z = \hat{E}_z(Ri, G, Q), \tag{74a}$$

$$\hat{F}_z = \hat{F}_z(Ri, G, Q), \tag{74b}$$

$$A_z = A_z(Ri, G, Q), \tag{74c}$$

[1] This result is very favourable. It allows us to fully separate the problems of the energy and flux budgets (considered in this paper) and the vertical turbulent length scale, l_z (to be considered later).

which can be found numerically. Other important dimensionless parameters of turbulence are expressed through $\hat{E}_z$, $\hat{F}_z$ and A_z:

$$Ri_f \equiv \frac{-\beta F_z}{\tau S} = \frac{\hat{F}_z}{2C_\tau}\left[1 + \frac{8C_\tau^2}{3\hat{E}_z} G\left(1 - \frac{4}{5Q}\right)\right], \tag{75}$$

$$\left(\frac{\tau}{E_K}\right)^2 \equiv \left(\frac{\tau_{13}^2 + \tau_{23}^2}{E_K}\right) = \frac{\hat{E}_z}{C_K^2}\left(1 - \frac{\hat{F}_z}{2C_\tau} + \frac{2G}{3}\left(A_z^{-1} + 3(Q-1)\right)\right)^{-2} \times \left[1 + \frac{8C_\tau^2}{3\hat{E}_z} G\left(1 - \frac{4}{5Q}\right)\right]^{-2}, \tag{76}$$

$$\frac{F_z^2}{E_K E_\theta} = \frac{2C_\tau A_z}{C_P \mathrm{Pr}_T}\left[1 + \frac{4C_F}{3\hat{F}_z} G\left(A_z^{-1} + 3(Q-1)\right)\right]^{-1}, \tag{77}$$

$$\frac{E_p}{E_K} = \frac{C_P}{2C_\tau C_K}\left[\hat{F}_z + \frac{4C_F}{3} G\left(A_z^{-1} + 3(Q-1)\right)\right] \times \left(1 - \frac{\hat{F}_z}{2C_\tau} + \frac{2G}{3}\left(A_z^{-1} + 3(Q-1)\right)\right)^{-1}. \tag{78}$$

In contrast with Eqs. 76–78, the vertical turbulent fluxes of momentum and potential temperature essentially depend on l_z:

$$\tau_{\alpha 3} = -K_M \frac{\partial U_\alpha}{\partial z}, \tag{79a}$$

$$K_M = 2C_\tau E_z^{1/2} l_z \left[1 + \frac{8C_\tau^2}{3\hat{E}_z} G\left(1 - \frac{4}{5Q}\right)\right]^{-1}, \tag{79b}$$

$$F_z = -K_H \frac{\partial \Theta}{\partial z}, \tag{80a}$$

$$K_H = \frac{K_M Ri_f}{Ri}, \tag{80b}$$

where Ri_f is determined by Eq. 75.

At $Ri \ll 1$, the above dimensionless parameters have precisely the same asymptotic limits as in our new EFB closure without IGW:

$$Pr_T \to Pr_T^{(0)} = \frac{C_\tau}{C_F}, \tag{81}$$

$$A_z \to A_z^{(0)} = \frac{C_r}{3(1 + C_r)}, \tag{82}$$

$$\left(\frac{\tau}{E_K}\right)^2 \to \frac{2C_\tau A_z^{(0)}}{C_K}, \tag{83}$$

$$\frac{F_z^2}{E_K E_\theta} \to \frac{2C_F A_z^{(0)}}{C_P}, \tag{84}$$

where the superscript "(0)" denotes $Ri \to 0$.

6 Comparison of the EFB + IGW Model with Empirical Data

Zilitinkevich et al. (2007) assumed that $C_P = C_K$ and determined the empirical coefficients C_r, C_K, C_F, C_τ (in op. cit. designated by Ψ_τ), and C_θ by comparison of results from the model with data from field and laboratory experiments, large-eddy simulations (LES) and direct numerical simulations (DNS) related to the asymptotic regimes at $Ri \ll 1$ and $Ri \gg 1$. For $Ri \ll 1$ we employ, in particular, the following estimates: $A_z^{(0)} = 1/6$ [after laboratory experiments on wall-bounded turbulence (L'vov et al. 2006) and DNS (Moser et al. 1999)], $(\tau/E_K)^{(0)} = 0.26$ and $[F_z^2(E_K E_\theta)^{-2}]^{(0)} = 0.11$ (after our comparative analyses of different data). The superscript (0) in the above notations means "at $Ri \ll 1$".

As already mentioned, we basically follow Zilitinkevich et al. (2007) but no longer assume that $C_P = C_K$. Then using the well-established empirical values of the turbulent Prandtl number, $Pr_T^{(0)} = 0.8$ (Elperin et al. 1996; Churchill 2002; Foken 2006), and the von Karman constant, $k_u = 0.4$, in the wall law $dU/dz = \tau^{1/2}(k_u z)^{-1}$ for the neutrally stratified surface layer (where $l_z \sim z$), the four constants are immediately obtained:

$$C_r = 3A_z^{(0)}(1 - 3A_z^{(0)})^{-1} = 1, \tag{85}$$

$$C_K = k_u (A_z^{(0)})^{1/2} \left[(\tau/E_K)^{(0)}\right]^{-3/2} = 1.2, \tag{86}$$

$$C_\tau = C_K (2A_z^{(0)})^{-1}(\tau^2/E_K^2)^{(0)} = 0.25, \tag{87}$$

$$C_F = C_\tau / \overset{(0)}{\mathrm{Pr}}_T = 0.31, \tag{88}$$

where we used Eqs. 81–84. Note that these estimates employ only data for neutrally stratified flows and therefore are equally relevant to the EFB and the EFB+IGW models because the IGW effects diminish at $Ri \ll 1$.

The maximal flux Richardson number for the flow without IGW, Ri_f^∞, and the ratio C_P/C_K can be roughly estimated using Eq. 7 in Zilitinkevich et al. (2008), which is derived from the budget equations for the kinetic and potential turbulent energies:

$$\frac{E_P}{E} = \frac{(C_P/C_K) Ri_f}{1 + (C_P/C_K - 1) Ri_f}. \tag{89}$$

Using the following values for the parameters $Ri_f^\infty = 0.2$ and $(E_P/E)^\infty = 0.15$ (see the thick solid line in Fig. 5 representing a median for different kinds of empirical data), and Eq. 89 we determined that

$$C_P/C_K = 0.72\,. \tag{90}$$

Because of a lack of better data, we consider this value of C_P/C_K,relevant to the regime without IGW.

It remains to determine the constant C_θ in Eq. 67. In the EFB closure without IGW, it is expressed through the limiting values of the energy ratio, A_z, and the flux Richardson number, Ri_f, at $Ri \to \infty$. Then, adopting reasonable values, $Ri_f^\infty = 0.2$ and $A_z^\infty = 0.056$, for the regime without IGW (solid lines in Figs. 2–5 based on the DNS, LES and laboratory experiments presumably unaffected by IGW), we obtain

$$C_\theta = \frac{A_z^\infty}{Ri_f^\infty}(1 - Ri_f^\infty) = 0.31, \tag{91}$$

where the superscripts "(0)" and "∞" denote "at $Ri = 0$" and "at $Ri \to \infty$", respectively.

Typical atmospheric values of the wave-energy parameter G, Eq. 50, and the lapse rate parameter Q, Eq. 44, determining the effects of IGW in our closure model, are estimated as follows. The first parameter, G, is obviously non-negative and in the Earth's troposphere could vary from zero (in the absence of waves) to about 10 in layers with strong wave activity. In the stratosphere G could be much larger, and IGW could become the major source of turbulence.

Since the IGW are trapped by the strongly stratified layers, we consider $N(z) \geq N(Z_0)$, that is $Q \geq 1$. Furthermore, the static stability of the troposphere varies only slightly around typical value of the Brunt–Väisälä frequency $N \approx 10^{-2}\,\mathrm{s}^{-1}$. Therefore, reasonable estimates for the orographically generated IGW are: $N(z) \approx N(Z_0) \approx 10^{-2}\,\mathrm{s}^{-1}$, and $Q = [N(z)/N(Z_0)]^2 \approx 1$. In the alternative case, when IGW propagating in the free troposphere are trapped by the stronger stratified long-lived stable planetary boundary layer, where $N^2 \approx 5(\beta F_z/\tau)^2 \mathrm{s}^{-2}$(e.g., Zilitinkevich and Esau 2007), Q could be a few times larger. A reasonable meteorological range of the lapse rate parameter is $1 < \mathrm{Q} < 5$.

In the EFB+IGW model the maximal flux Richardson number $Ri_f^{\max} \equiv (\lim Ri_f$ at $Ri \to \infty)$ is no longer a universal constant. Its variations are controlled by the counteraction of the direct and indirect mechanisms of generation of the turbulent flux of potential temperature by IGW, namely, by the two terms on the right-hand side (r.h.s.) of Eq. 26: "direct": $\Pi_F^w = -\left\langle F_j^w (\partial V_z^w/\partial x_j)\right\rangle_w$ and "indirect", caused by the temperature fluctuations: $C_\theta \beta \left\langle\theta^2\right\rangle = \beta\left\langle\theta^2\right\rangle + \rho_0^{-1}\left\langle\theta(\partial p/\partial z)\right\rangle$ (where $\left\langle\theta^2\right\rangle$ satisfies Eq. 23). As shown in Fig. 1, $Ri_f^{\max}$ with increasing G increases at $1 \leq Q < 1.02$, and decreases at $Q > 1.03$. Note that the maximal flux Richardson number $Ri_f^{\max}$ at $Q > 1.03$ reaches zero at some value of G (dependent on Q). For larger G the vertical flux of potential temperature becomes positive, that is counter-gradient. This looks surprising, but in fact is only natural. Indeed, IGW generate the potential temperature fluctuations, which in turn generate the upward (positive) contribution to the flux of potential temperature (cf. the above "indirect" mechanism). When the "indirect" share of the flux becomes larger than the "direct" share, the resulting flux changes sign and becomes positive in spite of the stable stratification.

Figures 2–5 show empirical data on the Ri dependences of the turbulent Prandtl number, Pr_T, flux Richardson number, Ri_f, energy–flux ratios, $(E_K/\tau)^2$ and $(E_K E_\theta)/F_z^2$, and energy ratios A_z and E_P/E together with theoretical curves plotted after the EFB model (heavy solid lines) and the EFB+IGW model for different G and Q. Since at $Ri < 0.25$, large-scale IGW practically do not affect turbulence, the model predictions accounting for IGW are plotted in Figs. 2–5 only for $Ri > 0.25$.

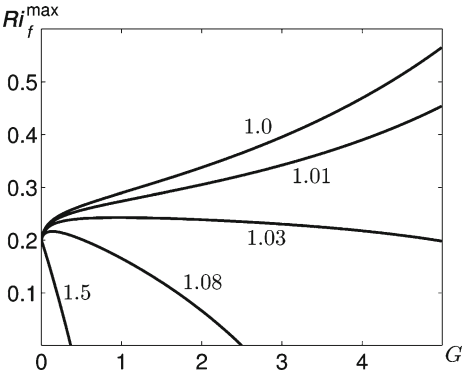

Fig. 1 Maximal values $Ri_f^{\max}$ (attainable at $Ri \to \infty$) of the flux Richardson number, $Ri_f = -\beta F_z(\tau S)^{-1}$, as functions of the wave energy parameter, G, Eq. 50, for different values of the lapse rate parameter, Q, Eq. 44

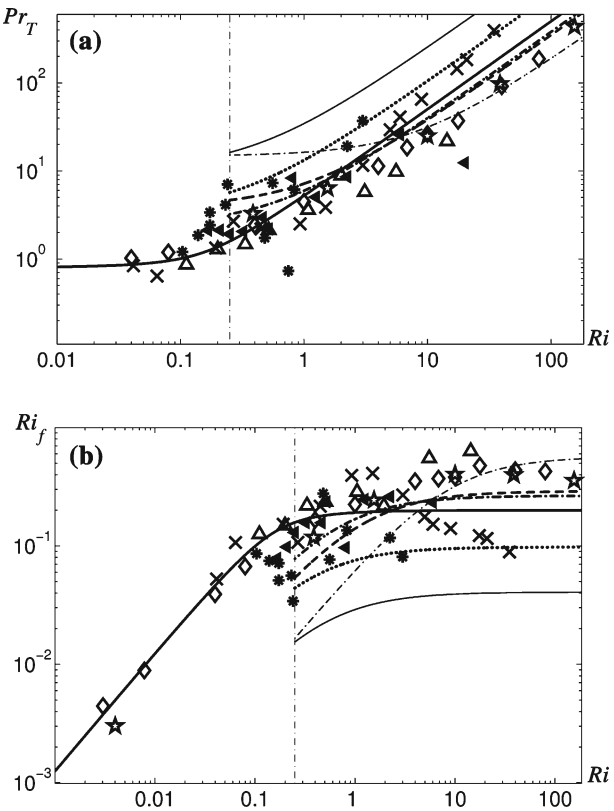

Fig. 2 Ri dependences of **a** turbulent Prandtl number, $Pr_T = K_M/K_H$, and **b** flux Richardson number, Ri_f. Data points show meteorological observations: *slanting black triangles* (Kondo et al. 1978), *snowflakes* (Bertin et al. 1997); laboratory experiments: *black circles* (Strang and Fernando 2001), *slanting crosses* (Rehmann and Koseff 2004), *diamonds* (Ohya 2001); LES: *triangles* (Zilitinkevich et al. 2008); and DNS: *five-pointed stars* (Stretch et al. 2001). *Curves* are plotted after our model (with $Ri_f^\infty = 0.2$): *thick solid lines* for the no-IGW regime ($G = 0$); *thin dashed-dotted lines* for $Q = 1$ and $G = 5$; *dashed lines* for $Q = 1$ and $G = 1$; *thick dashed-dotted lines* for $Q = 1$ and $G = 0.5$; *thin solid lines* for $Q = 1.5$ and $G = 0.3$; *dotted lines* for $Q = 1.5$ and $G = 0.2$

Recall that we consider the simplest version of our closure model relevant to the stationary homogeneous regime of turbulence (with no non-local sources turbulent energies or turbulent fluxes). On the contrary, most available empirical data represent vertically (and in some cases also horizontally) heterogeneous flows, controlled (besides Ri, G and Q) by additional, practically unavailable parameters. In this context, empirical Ri dependencies of Pr_T, Ri_f, $(\tau/E_K)^2$, $F_z^2/(E_K E_\theta)$, A_z and $E_P E_K^{-1}$ demonstrated by Mauritsen and Svensson (2007) and Zilitinkevich et al. (2007, 2008) are encouraging.

Below we attempt to more accurately determine empirical constants of the model. For this purpose, we rule out data suspicious because of strong heterogeneity, and limit our analyses to meteorological data of Kondo et al. (1978), Bertin et al. (1997), Banta et al. (2002), Poulos et al. (2002), Uttal et al. (2002) and Mahrt and Vickers (2005); laboratory data of Strang and Fernando (2001), Rehmann and Koseff (2004) and Ohya (2001); LES data of Esau (2004) and Zilitinkevich et al. 2008; and DNS data of Stretch et al. (2001).

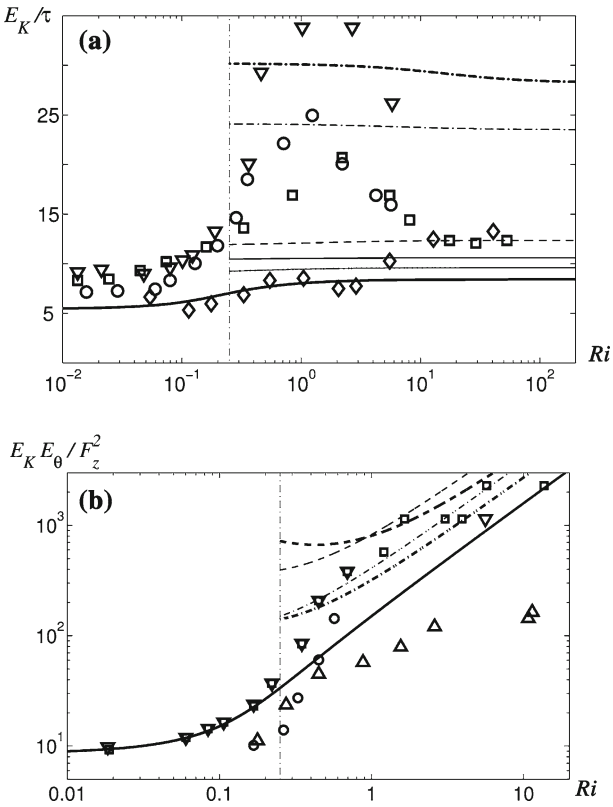

Fig. 3 Same as in Fig. 2 but for the energy to flux ratios: **a** $(E_K/\tau)^2$ and **b** $(E_K E_\theta)/F_z^2$. Data points show meteorological observations: *squares* [CME = Carbon in the Mountains Experiment, Mahrt and Vickers (2005)], *circles* [SHEBA = Surface Heat Budget of the Arctic Ocean, Uttal et al. (2002)], *overturned triangles* [CASES-99 = Cooperative Atmosphere–Surface Exchange Study, Poulos et al. (2002), Banta et al. (2002)]; laboratory experiments: *diamonds* (Ohya 2001); and LES: *triangles* (Zilitinkevich et al. 2008). *Thick solid lines* show the no-IGW version of the model ($G = 0$). *Other lines* are in (**a**): *thin dashed-dotted lines* for $Q = 1$ and $G = 8$, *dashed lines* for $Q = 1$ and $G = 1$, *thick dashed-dotted lines* for $Q = 1$ and $G = 0.5$, *thin solid lines* for $Q = 1.5$ and $G = 0.3$, *dotted lines* for $Q = 1.5$ and $G = 0.2$; and in (**b**): *thick dashed lines* for $Q = 1$ and $G = 0.4$, *thick dashed-dotted lines* for $Q = 1$ and $G = 0.1$, *thin dashed lines* for $Q = 1.5$ and $G = 0.1$, *thin dashed-dotted lines* for $Q = 1.5$ and $G = 0.05$

Empirical Ri dependencies of the turbulent Prandtl number, Pr_T, and flux Richardson number, Ri_f, are shown in Fig. 2 together with the two kinds of theoretical curves: heavy solid lines calculated neglecting IGW for $Ri_f^\infty = 0.2$; and bunches of thin lines calculated accounting for IGW (for different G and Q) in the interval $Ri \geq 0.25$. The latter cover the range of variability of presented data, which allows us to at least partially attribute the spread of data to the IGW mechanisms. The same format is used to show the energy to flux ratios: $(E_K/\tau)^2$ and $(E_K E_\theta)/F_z^2$ in Fig. 3; the energy ratios: $A_z = E_z/E_K$ and E_P/E in Figs. 4 and 5.

With increasing G, the theory predicts that $(E_K/\tau)^2$ and $(E_K E_\theta)/F_z^2$ increase and A_z decreases. This looks only natural: in contrast to the mean shear, generating only horizontal velocity fluctuations, IGW generate both horizontal and vertical fluctuations and directly contribute to A_z. Similarly, the energy ratio, E_P/E, increases with increasing G due to the

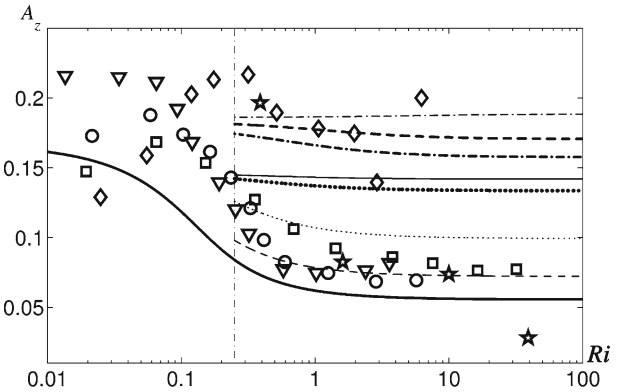

Fig. 4 Same as in Figs. 2 and 3 but for the energy ratio $A_z = E_z/E_K$ with additional DNS data of Stretch et al. (2001) shown by *five-pointed stars*. The theoretical curve for the no-IGW regime ($G = 0$) is shown by the *thick solid line*; other theoretical curves are: *thin dashed-dotted*, for $Q = 1$ and $G = 5$; *thick dashed*, for $Q = 1$ and $G = 1$; *thick dashed-dotted*, for $Q = 1$ and $G = 0.5$; *thin dotted*, for $Q = 1$ and $G = 0.05$; *thin dashed*, for $Q = 1$ and $G = 0.01$; *thin solid*, for $Q = 1.5$ and $G = 0.3$; *thick dotted*, for $Q = 1.5$ and $G = 0.2$

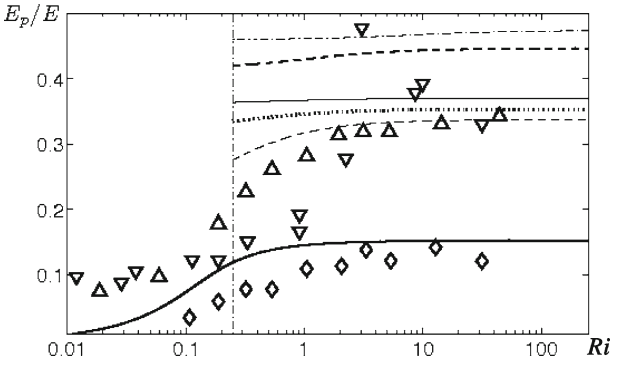

Fig. 5 The ratio of the potential to total turbulent energies, E_P/E, versus the gradient Richardson number, *Ri*. Data points show meteorological observations: *overturned triangles* [CASES-99 = Cooperative Atmosphere–Surface Exchange Study, Poulos et al. (2002), Banta et al. (2002)]; laboratory experiments: *diamonds* (Ohya 2001); and LES: *triangles* (Zilitinkevich et al. 2008). *Curves* are plotted after our model with $Ri_f^\infty = 0.2$: *thick solid line* for the no IGW regime ($G = 0$); *thin dashed-dotted line* for $Q = 1$ and $G = 5$; *thick dashed line* for $Q = 1$ and $G = 1$; *thick dashed-dotted line* for $Q = 1$ and $G = 0.5$; *thin dashed line* for $Q = 1$ and $G = 0.1$; *thin solid line* for $Q = 1.5$ and $G = 0.3$; *dotted line* for $Q = 1.5$ and $G = 0.2$

direct generation of turbulent potential energy by IGW. It is worth mentioning that Fig. 3b reveals the linear asymptote: $(E_K E_\theta)/F_z^2 \sim Ri$ at $Ri \gg 1$.

7 Concluding Remarks

In stably stratified atmospheric and oceanic flows, large-scale IGW directly perform vertical transport of momentum and contribute to TKE and TPE generation. Furthermore, the mean squared potential temperature fluctuation, $\langle\theta^2\rangle$, proportional to the TPE,

essentially controls the generation of the vertical turbulent flux of potential temperature, which is why this flux is also affected by IGW. In contrast to the mean shear, which directly generates only the horizontal component of TKE, large-scale IGW generate all three TKE components: E_x, E_y and E_z, and therefore essentially reduce anisotropy, that is increase the parameter $A_z = E_z/E_K$. This effect is especially pronounced in very stable stratification and quite probably represents the key source of a very large scatter in empirical plots of A_z versus Ri.

Furthermore, large-scale IGW generate both kinetic and potential turbulent energies and, as a rule, increase the share of the potential energy. Consequently, the maximal flux Richardson number ($Ri_f^{\max}$ attainable at $Ri \to \infty$) is no longer a universal constant (Ri_f^{∞}) as in the EFB model, but a variable parameter essentially dependent on both the IGW energy parameter G, Eq. 50, and the lapse rate parameter Q, Eq. 44. At different Q, this effect causes larger as well as smaller values of $Ri_f^{\max}$ (see Fig. 1). At $Q < 1.03$, the theory leaves room for the values of $Ri_f^{\max}$ exceeding 1 – obviously impossible in the stationary homogeneous flows without IGW, but observed in some experiments. On the contrary, at $Q > 1.03$ and sufficiently large values of the wave energy parameter, G, the maximal flux Richardson number, $Ri_f^{\max}$, reaches zero and then becomes negative, which means that the vertical flux of potential temperature, F_z, becomes positive, in spite of $\beta\partial\Theta/\partial z \equiv N^2 > 0$. The point is that IGW directly produce potential temperature fluctuations, which in turn produce the upward contribution to F_z. When it exceeds the contribution due to the potential temperature gradient, the resulting flux changes sign and becomes counter-gradient.

When the sources of IGW are located at the lower boundary of the air flow ($Z_0 = 0$), in particular, when IGW are generated by the flow interaction with mountains or hills, the vertical flux of momentum caused by IGW, $\tau_{\alpha 3}^{WW}$, is negative and contributes to the total (turbulent + wave induced) flux: $\tau_{\alpha 3} + \tau_{\alpha 3}^{WW} < 0$. This well-known mechanism is called "wave drag" (e.g., Nappo 2002).

When the source of IGW is located at the upper boundary of a strongly stratified atmospheric boundary layer trapping the IGW from the free atmosphere, Z_0 can be identified with the boundary-layer height. Then the velocity difference $U(z) - U(Z_0)$ is negative; and the wave-induced vertical flux of momentum, $\tau_{\alpha 3}^{WW}$, determined by Eq. 43 is oriented upwards: $\tau_{\alpha 3}^{WW} > 0$. It follows that $\tau_{\alpha 3}^{WW}$ counteracts the ordinary vertical turbulent flux of momentum, $\tau_{\alpha 3} < 0$, so that the total momentum flux and therefore the level of turbulence in the ABL diminish.

To the best of our knowledge, the above mentioned IGW mechanism leading to the counter-gradient heat transfer at large positive gradient Richardson numbers, as well as the upward transfer of momentum and consequent weakening of the boundary-layer turbulence by trapped IGW, have not been considered until present. The trapped-wave effect could form the basis for dangerous air pollution events and is therefore of practical interest.

It goes without saying that the above unexpected theoretical predictions call for empirical verification. Empirical constants of our turbulence closure model, the most important of which is Ri_f^{∞}, also need to be more carefully determined from field and laboratory experiments, DNS and LES.

Acknowledgements This work has been supported by the EC FP7 projects ERC PBL-PMES (No. 227915) and MEGAPOLI (No. 212520), and the Israel Science Foundation governed by the Israel Academy of Sciences (grant No. 259/07).

References

Baines PG (1995) Topographic effects in stratified flows. Cambridge University Press, New York, 482 pp

Banta RM, Newsom RK, Lundquist JK, Pichugina YL, Coulter RL, Mahrt L (2002) Nocturnal low-level jet characteristics over Kansas during CASES-99. Boundary-Layer Meteorol 105:221–252

Baumert H, Peters H (2004) Turbulence closure, steady state, and collapse into waves. J Phys Oceanogr 34:505–512

Baumert H, Peters H (2009) Turbulence closure: turbulence, waves and the wave-turbulence transition—part 1: vanishing mean shear. Ocean Sci 5:47–58

Beer T (1974) Atmospheric waves. Wiley, New York, 300 pp

Bertin F, Barat J, Wilson R (1997) Energy dissipation rates, eddy diffusivity, and the Prandtl number: an in situ experimental approach and its consequences on radar estimate of turbulent parameters. Radio Sci 32:791–804

Canuto VM, Minotti F (1993) Stratified turbulence in the atmosphere and oceans: a new sub-grid model. J Atmos Sci 50:1925–1935

Canuto VM, Cheng Y, Howard AM, Esau IN (2008) Stably stratified flows: a model with no Ri(cr). J Atmos Sci 65:2437–2447

Cheng Y, Canuto VM, Howard AM (2002) An improved model for the turbulent PBL. J Atmos Sci 59:1550–1565

Chimonas G (1999) Steps, waves and turbulence in the stably stratified planetary boundary layer. Boundary-Layer Meteorol 90:397–421

Churchill SW (2002) A reinterpretation of the turbulent Prandtl number. Ind Eng Chem Res 41:6393–6401

Einaudi F, Finnigan JJ (1993) Wave-turbulence dynamics in the stably stratified boundary layer. J Atmos Sci 50:1841–1864

Einaudi F, Finnigan JJ, Fua D (1984) Gravity wave turbulence interaction in the presence of a critical level. J Atmos Sci 41:661–667

Elperin T, Kleeorin N, Rogachevskii I (1996) Isotropic and anisotropic spectra of passive scalar fluctuations in turbulent fluid flow. Phys Rev E 53:3431–3441

Elperin T, Kleeorin N, Rogachevskii I, Zilitinkevich S (2002) Formation of large-scale semi-organized structures in turbulent convection. Phys Rev E 66:066305-1–066305-15

Elperin T, Kleeorin N, Rogachevskii I, Zilitinkevich S (2006) Turbulence and coherent structures in geophysical convection. Boundary-layer Meteorol 119:449–472

Esau I (2004) Simulation of Ekman boundary layers by large eddy model with dynamic mixed sub-filter closure. Environ Fluid Mech 4:273–303

Finnigan JJ (1988) Kinetic energy transfer between internal gravity waves and turbulence. J Atmos Sci 45:486–505

Finnigan JJ (1999) A note on wave-turbulence interaction and the possibility of scaling the very stable boundary layer. Boundary-Layer Meteorol 90:529–539

Finnigan JJ, Einaudi F (1981) The interaction between an internal gravity wave and the planetary boundary layer. Part II: effect of the wave on the turbulence structure. Q J Roy Meteorol Soc 107:807–832

Finnigan JJ, Einaudi F, Fua D (1984) The interaction between an internal gravity wave and turbulence in the stably-stratified nocturnal boundary layer. J Atmos Sci 41:2409–2436

Fofonoff NP (1969) Spectral characteristics of internal waves in the ocean. Deep-Sea Res 16:58–71

Foken T (2006) 50 years of the Monin–Obukhov similarity theory. Boundary-Layer Meteorol 119:431–447

Fritts DC, Alexander MJ (2003) Gravity wave dynamics and effects in the middle atmosphere. Rev Geophys 41(1):1003

Garrett C, Munk W (1979) Internal waves in the ocean. Annu Rev Fluid Mech 11:339–369

Gossard EE, Hooke WH (1975) Waves in the atmosphere. Elsevier, New York, 456 pp

Jacobitz FG, Rogers MM, Ferziger JH (2005) Waves in stably stratified turbulent flow. J Turbul 6:1–12

Jin LH, So RMC, Gatski TB (2003) Equilibrium states of turbulent homogeneous buoyant flows. J Fluid Mech 482:207–233

Kaimal JC, Fennigan JJ (1994) Atmospheric boundary layer flows. Oxford University Press, New York, 289 pp

Kolmogorov AN (1941) Energy dissipation in locally isotropic turbulence. Doklady AN SSSR 32(1):19–21

Kondo J, Kanechika O, Yasuda N (1978) Heat and momentum transfer under strong stability in the atmospheric surface layer. J Atmos Sci 35:1012–1021

Kurbatsky AF (2000) Lectures on turbulence. Novosibirsk State University Press, Novosibirsk, 118 pp

L'vov VS, Rudenko O (2008) Equations of motion and conservation laws in a theory of stably stratified turbulence. Phys Scr T132:014009-1–014009-5

L'vov VS, Pomyalov A, Procaccia I, Zilitinkevich SS (2006) Phenomenology of wall bounded Newtonian turbulence. Phys Rev E73:016303-1–016303-13
L'vov VS, Procaccia I, Rudenko O (2008) Turbulent fluxes in stably stratified boundary layers. Phys Scr T132:014010-1–014010-15
Mahrt L, Vickers D (2005) Boundary layer adjustment over small-scale changes of surface heat flux. Boundary-Layer Meteorol 116:313–330
Mauritsen T, Svensson G (2007) Observations of stably stratified shear-driven atmospheric turbulence at low and high Richardson numbers. J Atmos Sci 64:645–655
Mauritsen T, Svensson G, Zilitinkevich SS, Esau I, Enger L, Grisogono B (2007) A total turbulent energy closure model for neutrally and stably stratified atmospheric boundary layers. J Atmos Sci 64:4117–4130
Miropolsky YZ (1981) Dynamics of internal gravity waves in the ocean. Gidrometeoizdat, Leningrad, 302 pp (translation in English published in 2006)
Moser RG, Kim J, Mansour NN (1999) Direct numerical simulation of turbulent channel flow up to Re = 590. Phys Fluids 11:943–945
Nappo CJ (2002) An introduction to atmospheric gravity waves. Academic Press, London, 276 pp
Ohya Y (2001) Wind-tunnel study of atmospheric stable boundary layers over a rough surface. Boundary-Layer Meteorol 98:57–82
Pochapsky H (1972) Internal waves and turbulence in the deep ocean. J Phys Oceanogr 2:96–103
Polzin K (2004a) A heuristic description of internal wave dynamics. J Phys Oceanogr 34:214–230
Polzin K (2004b) Idealized solutions for the energy balance of the fine scale internal wave field. J Phys Oceanogr 34:231–246
Poulos GS, Blumen W, Fritts DC, Lundquist JK, Sun J, Burns SP, Nappo C, Banta R, Newsom R, Cuxart J, Terradellas E, Balsley B, Jensen M (2002) CASES-99: a comprehensive investigation of the stable nocturnal boundary layer. Bull Am Meteorol Soc 83:555–581
Rehmann CR, Koseff JR (2004) Mean potential energy change in stratified grid turbulence. Dyn Atmos Oceans 37:271–294
Rotta JC (1951) Statistische theorie nichthomogener turbulenz. Z Phys 129:547–572
Staquet C, Sommeria J (2002) Internal gravity waves: from instabilities to turbulence. Annu Rev Fluid Mech 34:559–593
Strang EJ, Fernando HJS (2001) Vertical mixing and transports through a stratified shear layer. J Phys Oceanogr 31:2026–2048
Stretch DD, Rottman JW, Nomura KK, Venayagamoorthy SK (2001) Transient mixing events in stably stratified turbulence. In: 14th Australasian fluid mechanics conference, Adelaide, Australia, 10–14 December
Thorpe SA (2004) Recent developments in the study of ocean turbulence. Annu Rev Earth Planet Sci 32:91–109
Turner JS (1973) Buoyancy effects in fluids. Cambridge University Press, Cambridge, 431 pp
Umlauf L, Burchard H (2005) Second-order turbulence closure models for geophysical boundary layers. A review of recent work. Cont Shelf Res 25:725–827
Uttal T, Curry JA, McPhee MG, Perovich DK et al (2002) Surface heat budget of the Arctic Ocean. Bull Am Meteorol Soc 83:255–276
Weinberg S (1962) Eikonal method in magnetohydrodynamics. Phys Rev 126:1899–1909
Wurtele MG, Sharman RD, Datta A (1996) Atmospheric lee waves. Annu Rev Fluid Mech 28:429–476
Zilitinkevich S (2002) Third-order transport due to internal waves and non-local turbulence in the stably stratified surface layer. Q J Roy Meteorol Soc 128:913–925
Zilitinkevich S, Esau I (2007) Similarity theory and calculation of turbulent fluxes at the surface for the stably stratified atmospheric boundary layers. Boundary-Layer Meteorol 125:193–296
Zilitinkevich SS, Elperin T, Kleeorin N, Rogachevskii I (2007) Energy- and flux budget (EFB) turbulence closure model for stably stratified flows. Part I: steady-state, homogeneous regimes. Boundary-Layer Meteorol 125:167–192
Zilitinkevich SS, Elperin T, Kleeorin N, Rogachevskii I, Esau I, Mauritsen T, Miles M (2008) Turbulence energetics in stably stratified geophysical flows: strong and weak mixing regimes. Q J Roy Meteorol Soc 134:793–799